Available online at www.sciencedirect.com
SCIENCE DIRECT®
International Journal of Multiphase Flow 30 (2004) 1193–1211
International Journal of Multiphase Flow
www.elsevier.com/locate/ijmulflow

# The influences of wave height on the interfacial friction in annular gas–liquid flow under normal and microgravity conditions

Zhaolin Wang, Kamiel S. Gabriel *, Devon L. Manz

*Microgravity Research Group, University of Saskatchewan, Saskatoon, Canada S7N 5A9*

Received 2 November 2002; received in revised form 19 June 2004

**Abstract**

In this paper, results for the interfacial friction factor and relative interfacial roughness on the gas–liquid interface are reported for an air–water annular flow in a small inner diameter tube (9.525 mm i.d.). The film structure was obtained through processing the time trace signal of film thickness that was measured using conductance probe technique. The interfacial friction factor and the relative interfacial roughness were altered through changing the gas mass flow rate. Changing gravity level was another way to alter the friction factor and roughness. It was found that wave height, hence the relative interfacial roughness (defined by the wave height measured from the substrate surface) decreased with increasing the gas Reynolds number. The roughness in microgravity is less than half of that in normal gravity, while the friction factor was about 10% smaller in microgravity than that in normal gravity. It was reasoned that the friction factor in annular two-phase flow decreased less significantly with the decrease of the relative interfacial roughness than that in single-phase flow, which could be explained by the flat wave shape in annular flow. The values of the interfacial shear stress at microgravity were also compared to those calculated at normal gravity. Based on the results, some similarities and differences between the single-phase flow and the gas core in annular flow were highlighted and discussed.


* Corresponding author. Present address: University of Ontario, Institute of Technology, 2000 Simcoe Street N., Oshawa, Ont., Canada L1H-7K4. Tel.: +1 905 721 3111; fax: +1 905 721 3140.
*E-mail address:* kamiel.gabriel@uoit.ca (K.S. Gabriel).

0301-9322/$ - see front matter © 2004 Elsevier Ltd. All rights reserved.
doi:10.1016/j.ijmultiphaseflow.2004.06.003

*Keywords:* Interfacial roughness; Wave height; Annular flow; Interfacial shear stress; Microgravity flow

## 1. Introduction

Numerous predictions of pressure drop in two-phase annular flow are currently available and although studies in this area have been active during the past few decades, the predictions only fit a specific range of conditions. The most widely used predictions of the pressure drop are based on methods adopted from single-phase flow, e.g. the Lockhart-Martinelli parameter (separated flow model). Therefore, if the pressure drop in annular two-phase flow is to be studied in a manner analogous to the single-phase model, both the similarities and differences between single-phase flow in a channel and annular flow with its distinct gas core and liquid annulus should be clearly understood before the single-phase flow method is adopted.

In comparison with single-phase flow, annular flow is characterized by the existence of a continuous gas core (which could be treated as a single-phase flow), and a distinctive gas–liquid interface. The gas–liquid interface usually depicts a complex structure consisting of dynamic and continuous interactions between the gas and liquid phases. As a result, the flow of each phase is inevitably influenced by the other phase. Mass and momentum transfers occur at the interface and greatly influence the pressure drop (Dukler and Fore, 1995).

It can be easily argued that the physical mechanism associated with the characteristics of a gas–liquid interface and the corresponding influence on the pressure drop are of vital importance to the study of two-phase annular flow. Unfortunately, until now and despite the fact that numerous correlations for the prediction of pressure drop in annular flow have been presented, few investigators have thoroughly examined the influence of the interfacial characteristics on the pressure drop.

As mentioned earlier, the gas–liquid interface in annular flow features interfacial waves. The characteristics of such waves include the interface structure itself (e.g. wave height, base height, spacing, etc.), as well as several important wave dynamic features (e.g. the wave speed, film speed, atomization and deposition rates), etc. Based on these characteristics, the gas phase could be regarded as a single-phase flow over a ''rough'' dynamic wavy interface, analogous to single-phase gas flow in a rough tube. In single-phase flow, the Reynolds number and the tube roughness are required to determine the interfacial shear stress. If a two-phase flow friction factor could be expressed in terms of the gas phase, an interface roughness is introduced as the analogous interfacial wave roughness height.

In some cases, the importance of the relative roughness was not recognized by previous investigators. Thus, the developed correlations were only applicable to a narrow range that corresponds to the experimental data. Theoretically speaking, the roughness could be determined from flow parameters such as the liquid Reynolds number and/or the mean film thickness. Consequently, some investigators used such parameters to indirectly infer a measure of the roughness. This could account for the complexity and diversity of the available models. The most relevant studies are summarized below.

Most investigators in this field would readily admit that the existence of interfacial waves in annular flow has a profound effect on the interfacial shear stress and hence the pressure drop. The earlier work of Wrobel and McManus (1961), modeled annular flow as a single-phase flow in a hydraulically rough pipe, and provided a theoretical basis for the interfacial roughness (representing the equivalent roughness in the single-phase model). In order to investigate the influence of the wave height on the pressure drop, Wrobel and McManus (1961) correlated the interfacial roughness with the friction factor. An accurate prediction of the pressure drop was made indicating that interfacial shear modeling will inevitably become more accurate through further knowledge of the wave structure and its random motion.

In addition, it was recognized that the presence of waves would influence the liquid atomization, which in turn could affect the mass and momentum transfer at the gas–liquid interface. Wrobel and McManus (1961) recognized in his early studies that the magnitude of the pressure drop could be orders of magnitude higher than the corresponding value for single-phase gas flow. They concluded that the increased pressure drop could be attributed to the large velocity gradients in the liquid film and the high form drag placed on the gas phase by the liquid film surface disturbances. As a result of the phase interaction, any attempt to analytically predict the film characteristics must include a study of the interfacial momentum transfer and the nature of the interface itself.

A similar observation was made by Henstock and Hanratty (1976). They indicated that the rough interface caused an increased drag on the liquid phase and resulted in a larger interfacial shear stress than that when the gas phase flows alone in a smooth channel. A correlation for the interfacial drag and the height of the wall layer was presented in their paper for an air–water system. Henstock and Hanratty (1976) referred to the work of previous researchers (Hewitt and Hall-Taylor, 1970) who suggested that the ratio of the two-phase interfacial stress to that for a smooth wall can be correlated by a length scale in terms of a ratio of the height of the film layer near the wall to the diameter of the tube. The model presented by Henstock and Hanratty (1976) was later modified by Asali et al. (1985). A correlation was presented for upward annular flow with negligible entrainment. They observed that the correlation failed as a result of wave reversal at gas velocities greater than 25 m/s.

In addition to the wave height, the wave spacing also influences the pressure drop. Asali and Hanratty (1993) analyzed the ripple waves and predicted the characteristic distance between the waves, further confirming the importance of the spacing in characterizing the interfacial stress in vertical gas–liquid annular flows. Moalem Maron and Brauner (1987) observed that the interfacial shear and pressure drop were directly related to the waviness of the film and the mobility of the interface. They evaluated the role of interfacial mobility, differentiating between the wavy film and the solid boundary. They also indicated that the interfacial shear stress is related to both the wave structure and the hydrodynamic features of the wave. They concluded that the difficulties in predicting the interfacial shear stress evolved from the complicated wave structure of the interface and the liquid entrainment and deposition processes.

As mentioned earlier, a fundamental understanding of the film structure is critical for better predictions of the pressure drop and heat transfer rates in annular two-phase flow. The literature contains a limited data set of pressure drop in microgravity. The work of Chen et al. (1991) and Colin et al. (1991) involved preliminary qualitative investigations into this topic for annular, bubble and slug flows. Chen et al. (1991), at a preliminary work, reported that the pressure drop in

normal gravity is related to the pressure drop in microgravity by the flow pattern models. From a very limited data set with R-113, they reported that the reduced gravity data had a larger pressure drop than the normal gravity data, which is rather surprising. Chen et al. (1991) also indicated that the database for microgravity two-phase flow patterns and pressure drop is very limited and hence accurate modeling was not possible at that time. Bousman (1995) collected pressure drop data in microgravity and compared the results with the Lockhart–Martinelli–Chisolm model (as presented in Whalley, 1987), and using a correlation presented in Wallis (1969). Using the limited data set, Bousman concluded that the Lockhart–Martinelli correlation was appropriate for calculating pressure drops at microgravity.

The majority of investigations on the interfacial shear stress rely on measurable average film characteristics such as the mean film thickness. Jayawardena and Balakotaiah (1996) observed the stability of wavy films in microgravity and normal gravity conditions. Commonly derived from time traces using averaging techniques, Balakotaiah has presented a theoretical justification for the use of wave features rather than time averaged values to accurately predict pressure drop in annular flow.

A relative velocity was used in the definition of the friction factor by Shearer and Nedderman (1965); among other investigators. This approach adds additional complication as it requires the estimation of an interfacial velocity. A dimensionless parameter, in terms of the film thickness to the diameter ratio, was used in a correlation presented earlier by Wallis (1970). The model contained the homogeneous core properties (rather than the gas properties) to better account for the effects of entrainment.

Since the interface structure greatly influences the pressure drop, it is reasoned that those factors influencing the interface structure would either directly or indirectly influence the pressure drop. The gravitational force is one of these factors. Many investigators such as Miles (2001), and Benjamin (1957) have theoretically examined the importance of the gravitational force on wave formation. As well, many investigators examined the direct contribution of the gravitational force to the pressure drop (Hughmark, 1973). However, few investigators have studied the indirect influence of the gravitational force on the pressure drop. Therefore, if the interface structure and pressure drop could be predicted in a microgravity environment, a profound understanding of the wave characteristics and its influence on the pressure drop would be achieved.

To further the investigation of the interfacial structure, detailed knowledge of the wave characteristics under both microgravity and normal gravity conditions were systematically studied by Zhu and Gabriel (2004). Their study provided a technique to accurately predict the interfacial characteristics and the influence on the pressure drop.

## 2. Instrumentation

Annular film flow is highly dynamic and as such the film characteristics (i.e., wave height, velocity, frequency, spacing, etc.) could be seen as random events as they fluctuate so rapidly. For our tube size and flow conditions, the average film thickness varies between 0.2 and 1.0 mm in a 9.53 mm ID tube. A high sampling rate and measurement accuracy are essential for a statistically sufficient representation of the film thickness. The parallel wire conductance probe, widely used by investigators (e.g., de Jong, 1999), measures the electrical conductance between two wires (40 μm

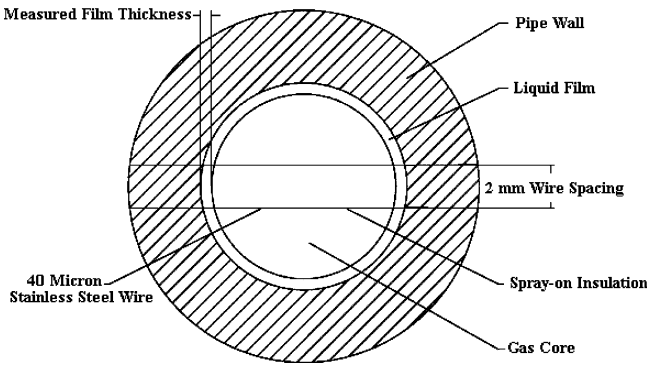


Fig. 1. A schematic of an individual film thickness probe (de Jong, 1999).

diameter) stretched across the channel cross-section. The film thickness probes were designed and built at the University of Saskatchewan. A schematic of the cross-sectional view is shown in Fig. 1. The principle of operation is based on measuring the electrical conductivity across the two-phase mixture to determine the relative amounts of gas and liquid. Water has a greater conductivity than air, and hence the amount of water in the tube can be determined from the conductivity measurement across the two wires (MacGillivray et al., 2001). Half of each wire is coated with an insulating varnish (GE no. 7031), thinned with a 50–50% solution of xylene and methanol so that measurements are taken over only half of the tube cross-section. Since the fully developed upward annular flow is examined, axial symmetry was assumed. This is done to avoid averaging by taking readings from one side of the tube.

The output of the film thickness probes were voltage signals. The probes were statically calibrated using the relationship between normalized output voltage and its corresponding value of controlled film thickness. The thickness of the film was simulated by the gap between two strictly coaxial cylinders. The inside cylinder was made of Teflon and was machined to tolerances of 0.02 mm. With changing the diameter of the inside cylinder, the film thickness was altered. The air (or liquid) flowed within the gap. The output voltage ($V_{\text{output}}$) of the film thickness was normalized using the equation: $V_{\text{normalized}} = (V_{\text{output}} - V_{\text{air}})/(V_{\text{water}} - V_{\text{air}})$; where $V_{\text{air}}$ and $V_{\text{water}}$ are the average output voltage of the probe for an air single-phase flow and a liquid single-phase flow in the gap, respectively. The normalized values were then plotted against the film thickness to produce the calibration curve from which the output voltage could be converted to the film thickness. Further details on the design and calibration of these sensors can be found in MacGillivray and Gabriel (2002).

A schematic of the flight loop is shown in Fig. 2. The two-phase mixture enters the test section (9.525 mm i.d. stainless steel tube, $D_t$), and develops over a length of 0.72 m ($76D_t$), where the first pressure tap is located. The gas loop consists of a cylinder of compressed air, a pressure regulator, a gas flow controller, and a check valve. The compressed gas is supplied from 50 litres cylinders at a pressure of 18 MPa. A pressure regulator is used to reduce the outlet pressure to approximately 500 kPa prior to the gas entering the mass flow controller. The gas mass flow rate is computer controlled via a 200 standard liters per minute gas mass controller. The gas is injected radially into the liquid through the mixing chamber, and after being separated in the separator tank, it is

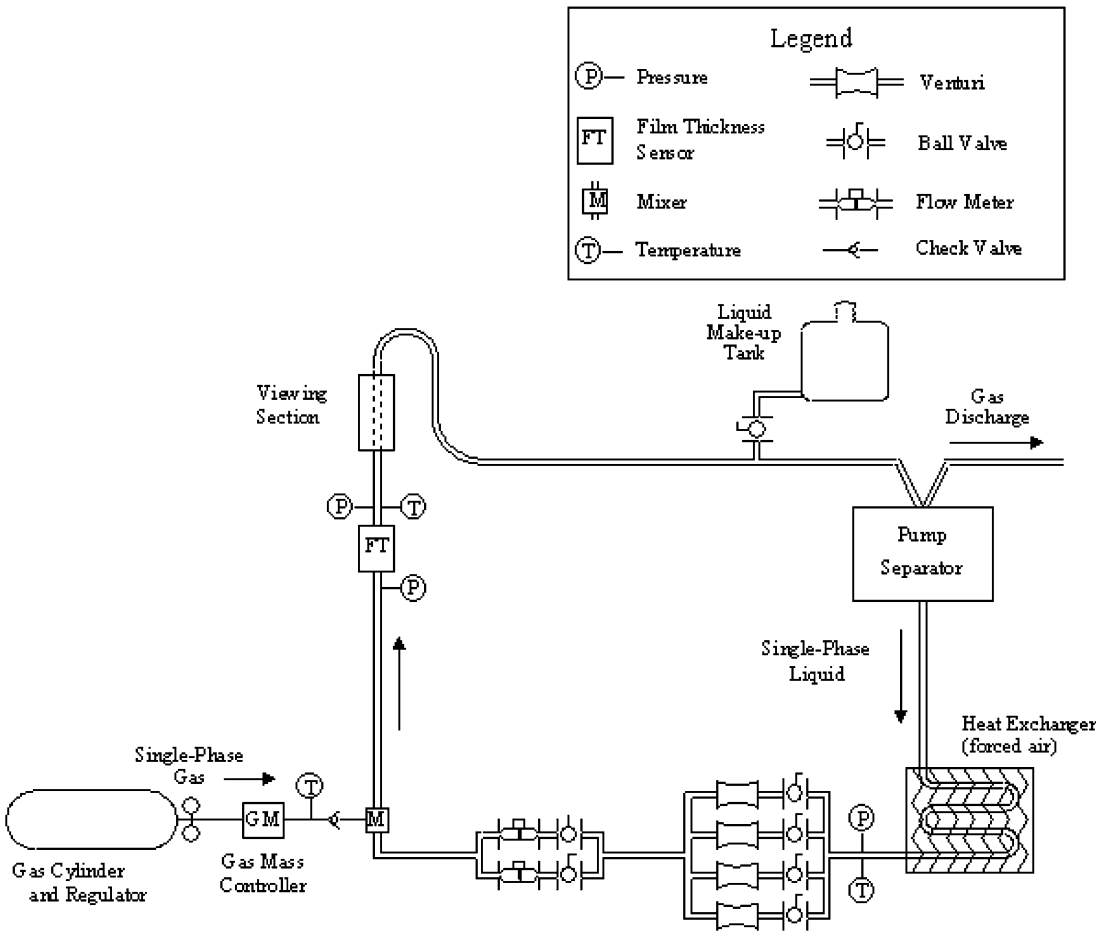


Fig. 2. A schematic of the flight experimental apparatus (MacGillivray et al., 2001).

vented to the surroundings during ground testing or vented overboard the airplane during flights that could provide microgravity environment for tens of seconds. Prior to the development of annular flow, the bubbling of air into the water through the porous wall of the mixer allows upward annular flow to develop naturally over the $76D_t$ developing length. The second pressure tap is located 0.88 m ($92D_t$) downstream the first tap. The differential pressure between the two taps was measured using a $\pm$ 2 psi diaphragm type pressure transducer. The first film thickness probe is located 1.44 m ($151D_t$) downstream the mixer, and the second probe is only 0.019 m ($2D_t$) downstream the first probe. The first film thickness probe was used in both the microgravity and normal gravity analysis to ensure that the wires in the first probe did not infringe on the film thickness measurements taken by the second probe. The system pressure was measured at the second pressure tap using a 50 psi absolute pressure transducer. Digital images of the flow were recorded through a solid acrylic viewing block using a 30 frames per second digital video camera at a position 0.13 m ($14D_t$) downstream of the second film thickness probe. This camera was used to provide a high resolution 2-D image for clarification of the flow pattern.

A computer based data acquisition and control system was implemented in the flight loop. The pump speed was controlled manually by adjusting a variable alternating current power source (VARIAC), while LabVIEW© controlled the remaining parameters. A 12-bit analog output board was used for control, and a 12-bit input board was used for the data acquisition. A 1024 Hz sampling rate was used for all data acquisition of gas and liquid temperatures and flow rates, pump speed, single-phase water pressure, film thickness measurements, pressure drop and the two-phase pressure and temperature. As analyzed by MacGillivray et al. (2001), the maximum total uncertainty was 0.104 mm for the film thickness measurements. Further details on experimental set up and instrumentation can be found in MacGillivray et al. (2001), and de Jong (1999).

Microgravity data was obtained during the 30th European Space Agency Microgravity Science Mission (May 2001) aboard the Zero-G Airbus 300, operated by Novespace out of Bordeaux, France. Initially the equipment was removed from the shipping crates and mounted to the frame in the appropriate positions, where inspection and leak tests were performed to verify tight connections and correct operation of the equipment. For the warm-up parabola, only water is circulated in the system, which established a reference point for the data. During the period of level flying between parabolas (approximately 1.5 min), the gas and liquid flow rates were adjusted to the desired point. This procedure was performed for each of the parabolas during the flight campaign. Many measurements were obtained, but of interest in this investigation were the film thickness time traces obtained in microgravity ($\sim$0.02 g) for air–water annular flows, and the ground data (1 g) which was later collected (April and May 2002) using the same flight campaign set points. A detailed experimental procedure was given by MacGillivray et al. (2001).

## 3. Wave characteristics

Since 1996, the development of a detailed interfacial wave structure has been the subject of extensive studies by the Microgravity Research Group at the University of Saskatchewan, Canada. The method used to reduce the film thickness time trace to an individual wave is described here and will be later used to determine the characteristics of the interfacial waves. A typical portion of a time trace for air–water flow at normal gravity (shown in Fig. 4a and b) features a series of wave peaks during a short window of data. In Fig. 3a, 0.20 s of the film thickness time trace distinctly reveals the wave peaks. Two seconds of a film thickness time trace is shown in Fig. 3b to illustrate the number of peaks during half of a typical time trace (four seconds). For the purpose of this analysis, a wave peak in a film thickness time trace was defined as any local maxima at least one standard deviation greater than the mean film thickness over the four second window of data. Since a high sampling rate was used during experimentation, this procedure eliminates the possibility of small waves that exist in the substrate being considered as waves. Between 80 and 150 such peaks were observed in a typical data analysis window. The time trace was divided into individual waves, which were then superimposed with alignment of the wave peak heights. The resulting *liquid peak height*, $H$, was determined as the average maximum height of the individual wave in the four seconds of data.

It is anticipated that atomization would strongly influence the wave structure and the pressure drop, hence for the flow examined in this investigation, the entrained fraction of the liquid less than 5% was studied so that the effects of the atomization on the wave amplitude and pressure

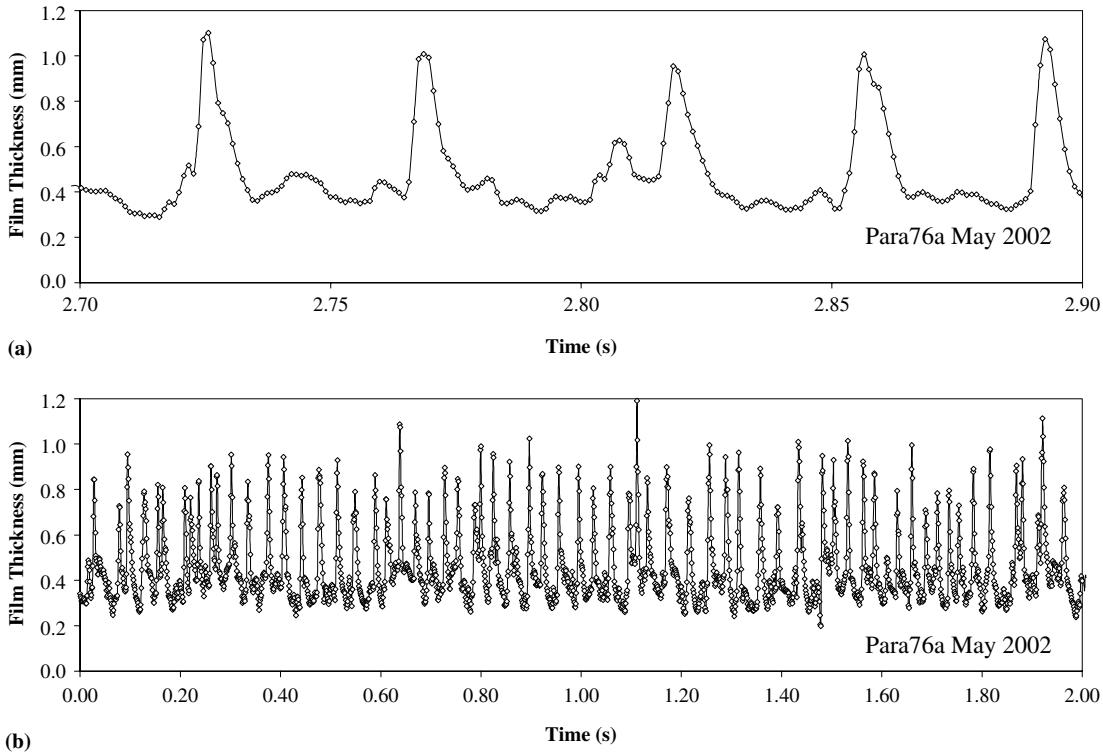


| $V_{sl}$ (m/s) | $V_{sg}$ (m/s) | $\dot{m}_g$ (g/s) | $\dot{m}_l$ (g/s) | ε (mm) |
|---|---|---|---|---|
| 0.120 | 24.3 | 2.24 | 8.52 | 0.059 |

Fig. 3. (a) Sample of a film thickness time trace (0.2 s, 1-g, para76a—May 2002); (b) sample of a film thickness time trace (2 s, 1-g, para76a—May 2002).

drop could be neglected. The conditions were controlled according to the experimental results of Han and Gabriel (2003), and Jepson et al. (1989). The same inside pipe diameter was adopted by Han and Gabriel and a 10.26 mm tube was used by Jepson et al. (1989). Under these conditions with negligible entrainment, the wave shape was obtained using the recorded time trace of the film thickness for each of the set points examined. The local wave peaks in the film thickness time trace were identified using the cutoff criterion initially described by de Jong (1999). The criterion was defined as the sum of the average film thickness and one standard deviation of the film thickness. In another parallel investigation by Zhu and Gabriel (2004), the CSD technique (cross-spectral density) was used to determine the wave velocity by measuring the time difference (corresponding to the same film height on one wave) using two pairs of film thickness probes separated by two tube diameters ($2D_t$). The local wave was calculated from the wave velocity and the traveling time of a point on the wave. Combined with the liquid height information of the local points on a wave, the wave shape as a function of the distance along the tube was finally determined.

From the above, a typical wave shape (for the same film thickness time trace shown in Fig. 4a and b) is featured in Fig. 4. The *starting point* of the average wave represents the first film

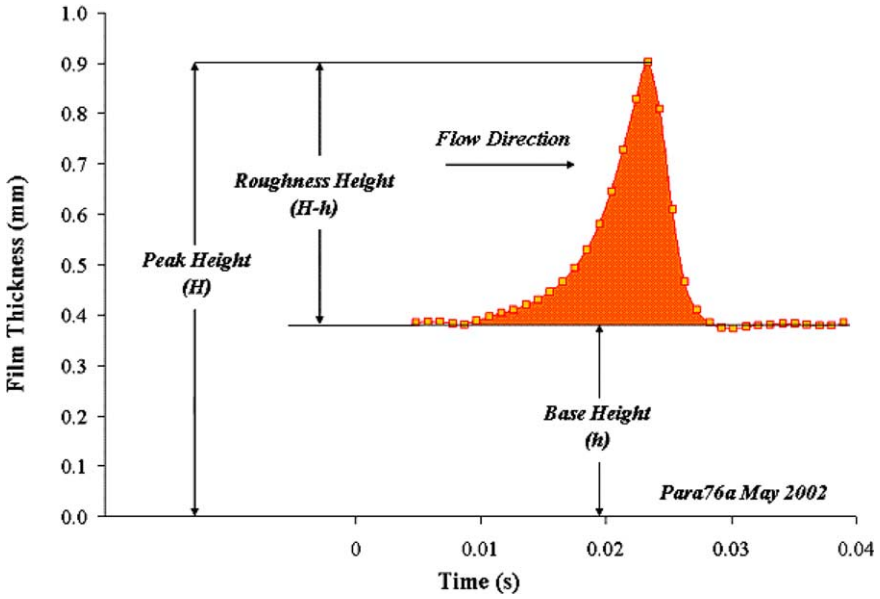


Fig. 4. Sample of an average wave shape (1-g, para76a—May 2002) (Zhu and Gabriel, 2004).

thickness value in the time trace that is greater than the wave base height by at least 5%. Conversely, the *ending point* is the last value in the film thickness time trace that is 5% greater than the following wave base height. The *liquid base height*, or the *substrate thickness*, $h$, is defined as the average value of the film thickness between the ending point of the previous average wave shape and the starting point of the current average wave shape. The *interfacial roughness height*, or the *wave height* ($H - h$), is defined as the difference between the liquid peak height and the liquid base height. Intuitively, the interfacial roughness height is the amplitude of the wave corresponding to the roughness of the tube wall in the single-phase model. The substrate surface corresponds to the tube wall in the single-phase flow model. Zhu and Gabriel (2004) also defined the *wave width*, the *wave spacing* and the *wave separation* to describe the relationship between two consecutive waves. The work of Zhu and Gabriel (2004) reported such features of the average wave shape based on the velocity of the wave. In this investigation, the wave width, wave spacing and wave separation were not considered in determining the friction factor.

It was shown (Zhu and Gabriel, 2004) that the parameters described above are influenced by the flow conditions as well as the fluid properties. Although the interfacial structure is dynamic, if the flow conditions and properties are certain, the interfacial structure should be predictable in a manner analogous to the roughness characteristics of a solid tube wall in single-phase flow. As a result, the interfacial structure and its influence on the interfacial friction could be studied in a comparable manner as with the single-phase model.

The wave structure at the air–water interface can be described by some dimensionless terms. The relative roughness is defined in terms of the interfacial roughness height divided by the hydraulic diameter of the gas core ($D_t - 2h$), i.e.

$$\varepsilon = \frac{H - h}{D_t - 2h} \tag{1}$$

The hydraulic diameter ($D_t - 2h$) was used rather than the inner tube diameter ($D_t$) because the gas phase flows over a gas–liquid interface rather than a solid wall. The roughness height ($H - h$) is adopted instead of the mean film thickness because it physically represents the shape of the interface. This way, the gas core flow could be treated more comparably with the single-phase flow.

The mean interfacial shear stress is also defined using a comparable form as with the single-phase pipe flow model. The length scale in the following equation defines the hydraulic diameter of the gas core rather than the inner tube diameter:

$$\frac{dP}{dz}_{\text{meas.}} \frac{\pi}{4}(D_t - 2h)^2 = \tau_i \pi (D_t - 2h) + \rho_g g \frac{\pi}{4}(D_t - 2h)^2 \tag{2}$$

where $\frac{dP}{dz}_{\text{meas.}}$ is the measured value of the pressure gradient. In deriving Eq. (2), the momentum change contributed by the transfer of liquid droplets is neglected due to the negligible entrainment. The negligible entrainment also accounts for the use of gas density rather than the use of gas-droplets mixture density. In Eq. (2), the accelerational pressure gradient (uniform cross section, no vapour expansion) was neglected and it is assumed that the measured pressure drop of the liquid film could represent the total pressure drop of the gas stream.

Eq. (2) can be further reduced to

$$\tau_i = \left(\frac{dP}{dz}_{\text{meas.}} - \rho_g g\right) \frac{(D_t - 2h)}{4} \tag{3}$$

The interfacial friction factor $C_f$, is defined from the interfacial shear stress $\tau_i$

$$C_f = \frac{2\tau_i}{\rho_g (V_g - V_i)^2} \tag{4}$$

where $V_g$ is the actual gas velocity, $V_i$ is the velocity of the gas–liquid interface. In our experiments, it was found that $V_i$ is usually less than 5% of $V_g$. Therefore, the friction factor can be well approximated by

$$C_f = \frac{2\tau_i}{\rho_g V_g^2} \tag{5}$$

## 4. Results and discussion

Approximately 25 microgravity and 50 normal gravity set points with gas mass flow rates ranging from 1.6 to 3.1 g/s were examined. The liquid mass flow rate ranged from 6.5 to 12.0 g/s. The data were reported earlier by MacGillivray and Gabriel (2002). In this study, the flow pattern map from Nedderman and Shearer (1963) was compared to the experimental results to determine the wave type. It was found that the wave type observed in this investigation was in the disturbance wave region.

### 4.1. The influence of changing the gas flow rate and gravity level on the interfacial roughness

Sample results of the wave shape at both normal and microgravity are shown in Fig. 5. The wave height is shown for a constant liquid flow rate ($\dot{m}_l \sim 7.85\ g/s$) at different gas flow rates. Fig. 5 shows a significant dependence of the wave height (i.e., interfacial roughness $H - h$) on the gas mass flow rate at both normal and microgravity. The interfacial roughness rapidly decreases with increasing the gas flow rate. For example, in normal gravity, when the gas mass flow rate increases from 1.64 to 3.35 g/s (104%), the roughness decreases by 58% (from 0.77 to 0.32 mm). The results are not surprising in that when the gas flow rate increases, the gas specific energy (hence the interfacial shear stress) increases as well. As a result, the "suppression" effect of the gas stream on the wave amplitude increases. Thus, the wave amplitude decreases with increasing the gas flow rate. This "suppression" effect was also reported earlier by other investigators (Asali and Hanratty, 1993; Sekoguchi et al., 1985; Nedderman and Shearer, 1963).

Fig. 5 also shows that gravity level exerts significant influence on the interfacial roughness. The roughness values in microgravity were less than half of the corresponding values in normal gravity at the same gas and liquid mass flow rates. This could be explained by the mechanism that gravitational force enhances the formation of waves. Under normal gravity condition, even if the velocity of the gas stream is relatively low, the effect of gravity will result in large waves generated by a number of complex mechanisms (as discussed in details by Benjamin, 1957; Clark et al., 1998). In microgravity, on the other hand, body forces due to gravitational acceleration are virtually eliminated. Therefore, we can argue that the wave height in microgravity is mainly determined by the forces exerted by the gas stream.

To study the friction factor, two dimensionless numbers are often employed: the surface relative roughness and the gas Reynolds number. Fig. 6a shows the dependence of the relative interfacial

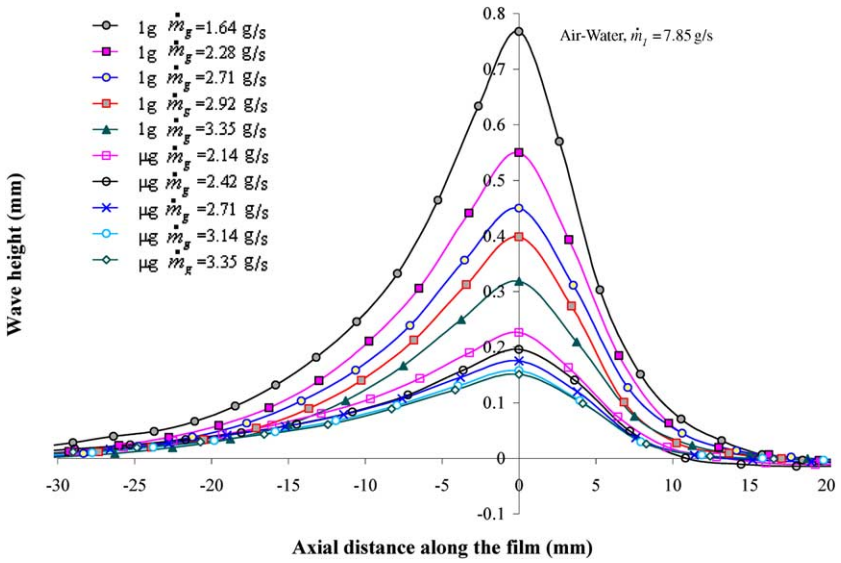


Fig. 5. Wave shape samples at 1 g and μg (Zhu and Gabriel, 2004).

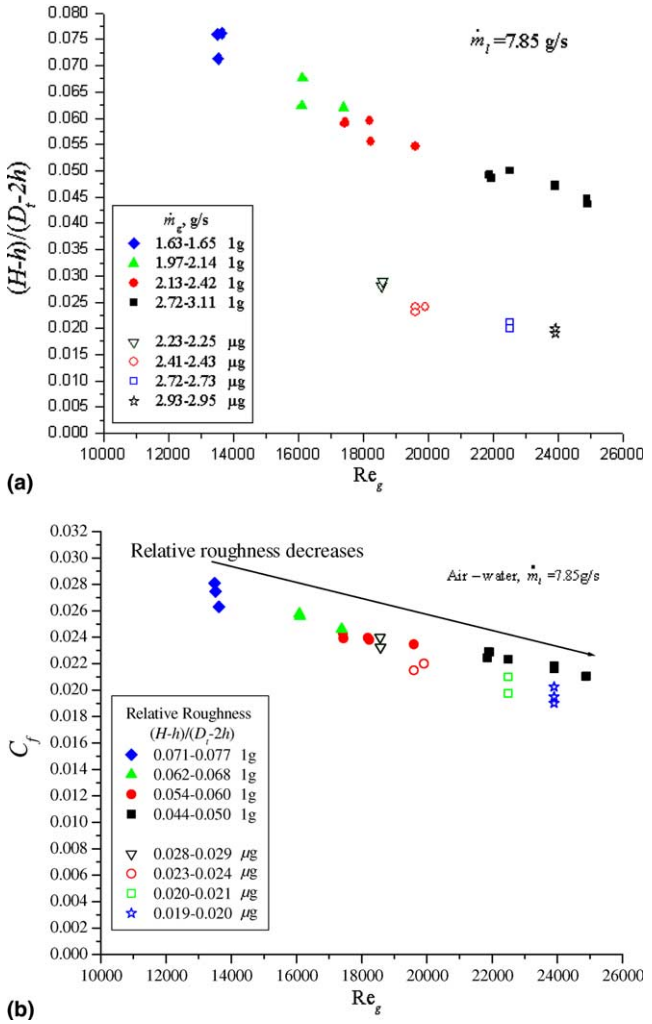


Fig. 6. The relationship of relative interfacial roughness, interfacial friction factor and gas Reynolds number.

roughness on the gas Reynolds number. For the gas phase flowing in the center of the tube, while the liquid phase is restricted to a thin film on the tube wall, the gas Reynolds number is calculated from

$$Re_g = \frac{(D_t - 2h)V_g\rho_g}{\mu_g} \tag{6}$$

where the term $D_t - 2h$ represents the hydraulic diameter of the gas stream.

Fig. 6a shows that the wave roughness dependence on the gravity level is very similar to that resulting from changing the gas mass flow rate. In summary, the relative interfacial roughness rapidly decreases with increasing the gas Reynolds number, and its values are less than half of the corresponding values in normal gravity. Since the substrate thickness $h$ is usually very small com-

pared to the tube diameter, the change in the substrate thickness has only a slight effect on the value of $(D_t - 2h)$. Therefore, a decrease in the wave height $(H - h)$, resulting from increasing the gas mass flow rate, will yield a corresponding decrease in the relative interfacial roughness $(H - h)/(D_t - 2h)$. In other words, the relative interfacial roughness will decrease with increasing the gas Reynolds number. It should be also pointed out that in annular two-phase flow, the interfacial roughness is a "dynamic" roughness, which is different from the normal wall roughness in single-phase flow.

Fig. 6a also illustrates that the amplitude of the relative roughness in normal gravity is larger than 0.045, and in microgravity the value is larger than 0.019. It is interesting to note that these values correspond to very rough surfaces, as shown on the Moody chart, for single-phase flow over rough surfaces (the maximum of the relative roughness published in most handbooks is about 0.05). This perhaps further illustrates the very dynamic nature of the disturbance waves in two-phase annular flows.

### 4.2. The effect of changing the gas flow rate and gravity level on the interfacial friction factor

In single-phase flow, an increase in the relative wall roughness causes a larger resistance to the gas stream. Consequently, the friction factor increases with the increase in the relative wall roughness (see Moody diagram). For the case in annular two-phase flow, Fig. 6b shows the change of friction factor with changing the relative interfacial roughness. The data points in Fig. 6b correspond to those in Fig. 6a. It can be found that the friction factor decreases with decreasing the relative roughness. One example is that in normal gravity, when the relative roughness decreases from 0.075 to 0.045 (40%), the friction factor decreases by 23% (from 0.0275 to 0.0211). However, this does not necessarily mean that the decrease of the friction factor is mainly caused by the decrease of the relative roughness. The results shown in Fig. 6b could also suggest that the decrease in the friction factor could be the result of increasing the gas Reynolds number, and hence the dependence of the friction factor on the roughness may not be as significant as the increased percentage (23%) may suggest. Furthermore, the dependence of the interface roughness on the gas Reynolds number makes it difficult to separately study their influences on the friction factor. Fortunately, as discussed earlier, the wave height strongly depends on the gravity level, and hence the gas Reynolds number and liquid mass flow rates could be controlled at different gravity levels. This way, the influence of the roughness on the friction factor could be separated from the influence of the gas Reynolds number.

Table 1 lists some typical values of the interfacial roughness and the friction factor. It can be seen that the friction factor in normal gravity is larger than that in microgravity gravity at the same gas Reynolds numbers and liquid mass flow rates. Also, when the relative roughness increases by more than 130% from μg to 1 g, the friction factor only increases by about 10%. Table 1 lists the corresponding increase in the friction factor in single-phase flow (assuming that the gas flows over a wall with the same roughness as of the gas–liquid interface, and with a similar gas Reynolds number of annular gas core). The friction factor values have been calculated using the widely accepted Colebrook equation for single-phase flow, as presented in (Gerhart and Gross, 1985):

Table 1
The values of interfacial roughness and friction factor ($\dot{m}_l = 7.85$ g/s)

| Experimental values of annular two-phase flow | | | | | | | Calculated values using single-phase flow equation | | |
|---|---|---|---|---|---|---|---|---|---|
| $Re_g$ | $\varepsilon_{\mu g}$ | $\varepsilon_{l\,g}$ | $(\varepsilon_{l\,g}-\varepsilon_{\mu g})/\varepsilon_{\mu g}$ (%) | $C_f^{\mu g}$ | $C_f^{l\,g}$ | $(C_f^{l\,g}-C_f^{\mu g})/C_f^{\mu g}$ (%) | $C_f^{\mu g}$ | $C_f^{l\,g}$ | $(C_f^{l\,g}-C_f^{\mu g})/C_f^{\mu g}$ (%) |
| 15,800 | 0.028 | 0.066 | 136.5 | 0.027 | 0.030 | 10.3 | 0.014 | 0.021 | 44.5 |
| 15,800 | 0.028 | 0.067 | 138.6 | 0.027 | 0.030 | 9.2 | 0.014 | 0.021 | 44.8 |
| 19,600 | 0.024 | 0.057 | 138.8 | 0.023 | 0.025 | 8.8 | 0.013 | 0.019 | 43.2 |
| 22,250 | 0.020 | 0.049 | 146.1 | 0.021 | 0.023 | 9.0 | 0.013 | 0.018 | 43.2 |
| 22,250 | 0.020 | 0.049 | 143.6 | 0.020 | 0.023 | 15.8 | 0.013 | 0.018 | 42.2 |
| 23,900 | 0.019 | 0.047 | 149.0 | 0.020 | 0.022 | 10.9 | 0.012 | 0.018 | 43.4 |
| 23,900 | 0.019 | 0.047 | 135.2 | 0.020 | 0.022 | 7.8 | 0.013 | 0.018 | 40.5 |

$$\frac{1}{\sqrt{f_i}} = -2.0\log\left(\frac{\varepsilon}{3.7}+\frac{2.51}{Re_g\sqrt{f_i}}\right) \tag{7}$$

$$C_f = \frac{f_i}{4} \tag{8}$$

where the relative roughness $\varepsilon$ was calculated using Eq. (1), and the gas Reynolds number $Re_g$ was calculated from Eq. (6).

It can be seen that the increase in the friction factor values (calculated using the single-phase flow equation) is more than 40%, which is four times the corresponding increase in annular gas-core flow. In other words, the dependence of the friction factor on the interfacial roughness in annular flow is less significant than that in single-phase flow. This is a surprising finding as the amplitude of the relative interfacial roughness in annular two-phase flow corresponds to very rough surface.

One explanation to offer here is that the friction factor may not be solely influenced by the roughness height, and that the roughness shape (in the case of interfacial flows) plays a significant role. As shown earlier in Fig. 5, the waves are relatively "flat", and the ratio of the wave height to the wave width ranges from 1:40 to 1:50. Sekoguchi et al. (1985) reported similar values of the same ratio. Flat waves are very likely to induce small form drag. It then follows that the friction factor in annular flow would most likely be less influenced by the interfacial roughness than in the case of single-phase flow over a rough surface.

From the less significant difference (about 10%) between the microgravity and normal gravity friction factors, it can be reasoned from Eq. (5) that the gas velocity, and hence the gas Reynolds number, have a predominant role in determining the magnitude of the interfacial shear stress. The calculated values of the interfacial shear stress are shown in Fig. 7, and the results clearly support this conclusion. It is an interesting phenomenon that some values of the interfacial shear stress in microgravity are even larger than those in normal gravity at the same gas and liquid mass flow rates. This is attributed to the higher gas core velocity in microgravity caused by the smaller gas core diameter.

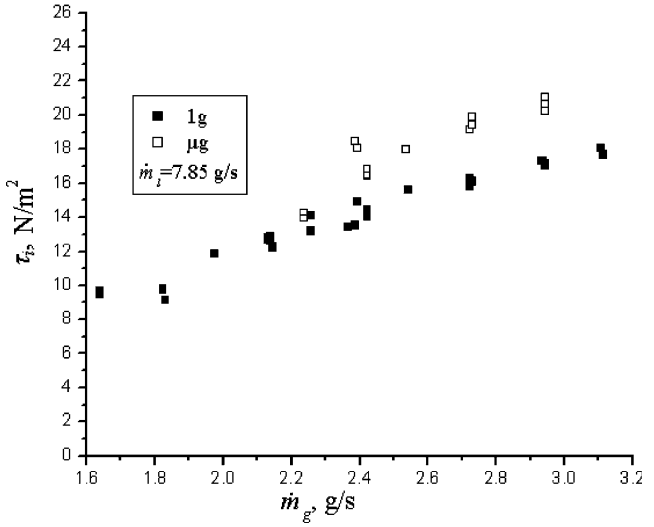


Fig. 7. The interfacial shear stress against gas mass flow rate.

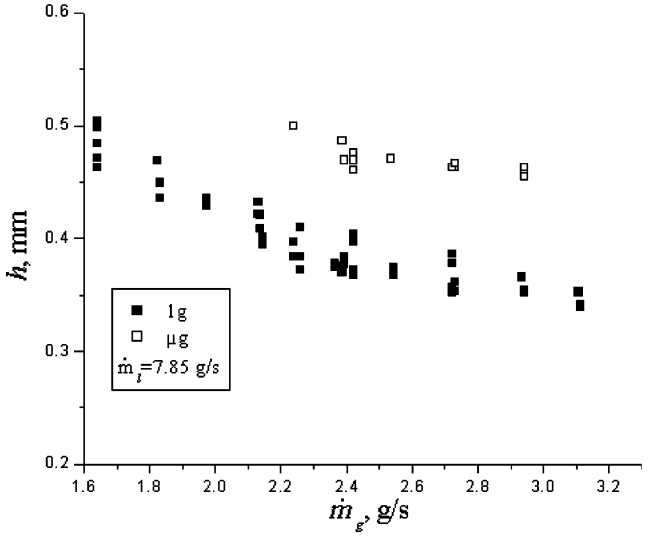


Fig. 8. The dependence of substrate thickness on the gas mass flow rate.

Finally, Fig. 8 shows the experimental values of the substrate thickness at different gravity levels. As seen, the substrate thickness in microgravity is larger than that in normal gravity, which will lead to a narrower gas core in microgravity (when the gas and liquid mass flow rates are kept the same). The thicker substrate in microgravity results from the smaller wave amplitude. This was shown earlier in Fig. 5. Smaller waves carry less liquid mass which in turn means that, for the same liquid mass floew rates, the substrate will carry more liquid and hence is thicker in microgravity. This has been systematically studied and reported by Zhu and Gabriel (2004).

## 5. Conclusions

(1) The wave height and relative interfacial roughness decrease with increasing the gas Reynolds number, indicating that the interfacial roughness in annular two-phase flow is dynamic.
(2) The wave height and the relative interfacial roughness in microgravity are less than half of the corresponding values in normal gravity.
(3) The relative interfacial roughness of annular two-phase flow in normal gravity are usually larger than the relative wall roughness covered by the single-phase Moody chart, and the chart only covers part of the interfacial roughness range in microgravity.
(4) The interfacial friction factor in annular two-phase flow increases with increasing the interfacial roughness, and decreases with increasing the gas Reynolds number. This is similar to the case in single-phase flow.
(5) In the gas core of annular flow, the roughness is dynamic and depends on the gas Reynolds number, which is different from the case in single-phase flow with constant roughness that is independent of the gas Reynolds number. This would bring difficulty to study the interfacial friction factor of the two-phase flow in a way similar to that indicated by single-phase flow Moody chart.
(6) The friction factor in annular flow is less significantly influenced by the interfacial roughness than that in single-phase flow. This could be accounted for by the "flat" wave shape. The ratio of the wave height to the wave width is from 1:40 to 1:50.
(7) The interfacial shear stress in microgravity is close to or even larger than that in normal gravity at the same gas and liquid mass flow rates, which could be attributed to two reasons: (a) the insignificant difference (about 10%) in the friction factors between microgravity and normal gravity; (b) the gas velocity in microgravity is higher than that in normal gravity. This is caused by the thicker substrate's thickness in microgravity.

## Acknowledgments

This project was co-sponsored by the Natural Sciences and Engineering Research Council of Canada (NSERC), and the Canadian Space Agency. We acknowledge the superb support that was received from the European Space Agency and Novespace during the parabolic flight campaigns in November 2000 and May 2001.

## Appendix A. Film thickness data

This appendix tabulates the wave characteristics presented in this paper. Table A.1 contains the normal gravity data, while Table A.2 contains the microgravity data. All microgravity data were collected in May 2001 and the normal gravity data were collected in April and May 2002.

Table A.1
Normal gravity film thickness

| $V_{sl}$ (m/s) | $V_{sg}$ (m/s) | $x$ | $\varepsilon$ |
|---|---|---|---|
| 0.108 | 28.4 | 0.287 | 0.045 |
| 0.114 | 28.4 | 0.277 | 0.045 |
| 0.114 | 28.4 | 0.278 | 0.045 |
| 0.110 | 27.9 | 0.273 | 0.047 |
| 0.115 | 27.9 | 0.264 | 0.047 |
| 0.110 | 27.9 | 0.274 | 0.047 |
| 0.115 | 27.9 | 0.265 | 0.048 |
| 0.110 | 26.8 | 0.259 | 0.049 |
| 0.109 | 26.9 | 0.261 | 0.049 |
| 0.110 | 26.8 | 0.259 | 0.049 |
| 0.114 | 26.8 | 0.251 | 0.049 |
| 0.109 | 26.9 | 0.260 | 0.050 |
| 0.104 | 25.4 | 0.244 | 0.051 |
| 0.114 | 26.9 | 0.251 | 0.052 |
| 0.107 | 25.3 | 0.241 | 0.053 |
| 0.103 | 25.2 | 0.244 | 0.053 |
| 0.104 | 25.2 | 0.243 | 0.054 |
| 0.108 | 25.3 | 0.240 | 0.055 |
| 0.104 | 25.4 | 0.244 | 0.055 |
| 0.093 | 24.0 | 0.245 | 0.055 |
| 0.119 | 25.2 | 0.221 | 0.055 |
| 0.121 | 26.2 | 0.218 | 0.055 |
| 0.114 | 25.4 | 0.230 | 0.056 |
| 0.122 | 25.8 | 0.216 | 0.056 |
| 0.119 | 25.2 | 0.220 | 0.057 |
| 0.113 | 25.5 | 0.231 | 0.058 |
| 0.113 | 23.7 | 0.210 | 0.059 |
| 0.111 | 24.1 | 0.214 | 0.059 |
| 0.128 | 23.5 | 0.190 | 0.060 |
| 0.093 | 24.0 | 0.244 | 0.060 |
| 0.113 | 23.6 | 0.209 | 0.060 |
| 0.107 | 23.7 | 0.219 | 0.061 |
| 0.129 | 23.5 | 0.189 | 0.062 |
| 0.107 | 23.7 | 0.219 | 0.062 |
| 0.107 | 23.7 | 0.219 | 0.062 |
| 0.112 | 24.1 | 0.212 | 0.062 |
| 0.092 | 21.5 | 0.217 | 0.063 |
| 0.104 | 19.7 | 0.198 | 0.067 |
| 0.100 | 21.1 | 0.199 | 0.067 |
| 0.092 | 21.5 | 0.216 | 0.068 |
| 0.099 | 21.1 | 0.200 | 0.069 |
| 0.101 | 18.1 | 0.204 | 0.071 |
| 0.101 | 18.2 | 0.203 | 0.071 |
| 0.145 | 21.6 | 0.152 | 0.071 |
| 0.104 | 19.7 | 0.198 | 0.071 |
| 0.110 | 19.7 | 0.173 | 0.071 |
| 0.145 | 21.6 | 0.152 | 0.072 |

(*continued on next page*)

Table A.1 (*continued*)

| $V_{sl}$ (m/s) | $V_{sg}$ (m/s) | $x$ | $\varepsilon$ |
|---|---|---|---|
| 0.111 | 19.7 | 0.172 | 0.076 |
| 0.112 | 19.9 | 0.171 | 0.076 |
| 0.116 | 18.1 | 0.166 | 0.080 |
| 0.115 | 18.1 | 0.168 | 0.080 |

Table A.2
Microgravity film thickness

| $V_{sl}$ (m/s) | $V_{sg}$ (m/s) | $x$ | $\varepsilon$ |
|---|---|---|---|
| 0.112 | 34.1 | 0.270 | 0.019 |
| 0.112 | 34.1 | 0.270 | 0.019 |
| 0.111 | 33.8 | 0.271 | 0.020 |
| 0.151 | 34.8 | 0.197 | 0.020 |
| 0.110 | 34.1 | 0.259 | 0.020 |
| 0.109 | 32.8 | 0.261 | 0.020 |
| 0.136 | 30.4 | 0.211 | 0.021 |
| 0.110 | 33.8 | 0.259 | 0.021 |
| 0.152 | 34.7 | 0.197 | 0.021 |
| 0.121 | 29.4 | 0.209 | 0.022 |
| 0.119 | 30.5 | 0.220 | 0.022 |
| 0.121 | 29.2 | 0.208 | 0.023 |
| 0.109 | 29.4 | 0.239 | 0.023 |
| 0.109 | 29.7 | 0.239 | 0.024 |
| 0.120 | 30.9 | 0.219 | 0.024 |
| 0.109 | 29.8 | 0.239 | 0.024 |
| 0.144 | 27.1 | 0.181 | 0.027 |
| 0.155 | 25.4 | 0.151 | 0.027 |
| 0.150 | 24.8 | 0.156 | 0.028 |
| 0.120 | 24.2 | 0.208 | 0.028 |
| 0.120 | 24.4 | 0.208 | 0.029 |
| 0.123 | 24.2 | 0.204 | 0.029 |
| 0.161 | 23.1 | 0.169 | 0.030 |
| 0.157 | 23.8 | 0.152 | 0.031 |
| 0.156 | 23.6 | 0.153 | 0.033 |

## References

Asali, J.C., Hanratty, T.J., 1993. Ripples generated on a liquid film at high gas velocities. Int. J. Multiphase Flow 19, 229–243.

Asali, J.C., Hanratty, T.J., Andreussi, P., 1985. Interfacial drag and film height for vertical annular flow. AIChE J. 31, 895–902.

Benjamin, T.B., 1957. Wave formation in laminar flow down an inclined plane. J. Fluid Mech. 2, 554–574.

Bousman, W.S., 1995. Studies of two-phase gas–liquid flow in microgravity. NASA Contractor Report 195434.

Chen, I., Downing, R., Keshock, E.G., Al-Sharif, M., 1991. Measurements and correlation of two-phase pressure drop under microgravity condition. J. Thermophys. 5, 514–523.

Clark, W.W., Hills, J.H., Azzopardi, B.J., 1998. The interfacial characteristics of falling film reactors. In: Proceedings Presented at the IChemE Research Event, NewCastle, 1998.

Colin, C., Fabre, J., Dukler, A.E., 1991. Gas–liquid flow at microgravity conditions—I. Dispersed bubble and slug flow. Int. J. Multiphase Flow 17, 533–544.

de Jong, P., 1999. An investigation of film structure and pressure drop in microgravity annular flow. M.Sc. Thesis, University of Saskatchewan, Canada.

Dukler, A.E., Fore, L.B., 1995. Droplet deposition and momentum transfer in annular flow. AIChE 41, 2040–2046.

Gerhart, P.M., Gross, R.J., 1985. Fundamentals of fluid mechanics. Addison-Wesley Publishing Company, Inc., Reading, MA, pp. 421–431.

Han, H.W., Gabriel, K.S., in preparation. Entrainment fraction measurement and its results analyses of annular two-phase upward flow in small diameter Tube.

Henstock, W.H., Hanratty, T.J., 1976. The interfacial drag and the height of the wall layer in annular flows. AIChE 22, 990–999.

Hewitt, G.F., Hall-Taylor, N.S., 1970. Annular two-phase flow. Pergamon Press, Oxford.

Hughmark, G.A., 1973. Film thickness, entrainment, and pressure drop in upward annular and dispersed flow. AIChE 19, 1062–1065.

Jayawardena, S.S., Balakotaiah, V., 1996. Stability of wavy films in gas–liquid two-phase flows at normal and microgravity conditions. In: Proceedings of 3rd Microgravity Fluid Physics Conference.

Jepson, D.M., Azzopardi, B.J., Whalley, P.B., 1989. The effect of gas properties on drops in annular flow. Int. J. Multiphase Flow 15, 327.

MacGillivray, R.M., Gabriel, K.S., 2002. A study of annular flow film characteristics in microgravity and hypergravity conditions. In: Proceedings of the 53rd International Astronautical Conference (under review).

MacGillivray, R.M., Leislar, T.J., Gabriel, K.S., 2001. The effect of gravity on annular two-phase flow. Final Report to the Canadian Space Agency, November, 2001.

Miles, J.W., 2001. Gravity waves on shear flows. J. Fluid Mech. 443, 293–299.

Moalem Maron, D., Brauner, N., 1987. The role of interfacial mobility in determining the interfacial shear factor in two-phase wavy film flow. Int. Commun. Heat Mass Transfer 14, 45–55.

Nedderman, R.M., Shearer, C.J., 1963. The motion and frequency of large disturbance waves in annular two-phase flow of air–water mixtures. Chem. Eng. Sci. 18, 661–670.

Sekoguchi, K., Takeishi, M., Ishimatsu, T., 1985. Interfacial structure in vertical upward annular flow. PCH PhysicoChem. Hydrodyn. 6 (1/2), 239–255.

Shearer, C.J., Nedderman, R.M., 1965. Pressure gradient and liquid film thickness in co-current upwards flow of gas/liquid mixtures: application to film-cooler design. Chem. Eng. Sci. 20, 671–683.

Wallis, G.B., 1970. Annular two-phase flow—part 1: a simple theory. J. Basic Eng. 92, 59–72.

Wallis, G.B., 1969. One dimensional two-phase flow. McGraw-Hill, New York.

Whalley, P.B., 1987. Boiling, Condensation and Gas–Liquid flow. Clarendon Press, Oxford.

Wrobel, J.R., McManus, H.N., 1961. An analytic study of film depth, wave height, and pressure drop in annular two-phase flow. Develop. Mech. 1, 578–587.

Zhu, Z., Gabriel, K.S., 2004. A study on the effect of gas flow rate on the wave characteristics in two-phase gas–liquid annular flow. Nuclear Engng. & Design (under review).